

A Journal of the Gesellschaft Deutscher Chemiker

# Angewandte Chemie

GDCh

International Edition

[www.angewandte.org](http://www.angewandte.org)

## Accepted Article

**Title:** Conductive Two-Dimensional Phthalocyanine-based Metal-Organic Framework Nanosheets for Efficient Electroreduction of CO<sub>2</sub>

**Authors:** Rong Cao, Jun-Dong Yi, Duan-Hui Si, RuiKuan Xie, Qi Yin, Meng-Di Zhang, Qiao Wu, Guo-Liang Chai, and Yuan-Biao Huang

This manuscript has been accepted after peer review and appears as an Accepted Article online prior to editing, proofing, and formal publication of the final Version of Record (VoR). This work is currently citable by using the Digital Object Identifier (DOI) given below. The VoR will be published online in Early View as soon as possible and may be different to this Accepted Article as a result of editing. Readers should obtain the VoR from the journal website shown below when it is published to ensure accuracy of information. The authors are responsible for the content of this Accepted Article.

**To be cited as:** *Angew. Chem. Int. Ed.* 10.1002/anie.202104564

**Link to VoR:** <https://doi.org/10.1002/anie.202104564>

# Conductive Two-Dimensional Phthalocyanine-based Metal-Organic Framework Nanosheets for Efficient Electroreduction of CO<sub>2</sub>

Jun-Dong Yi,<sup>[a]</sup> Duan-Hui Si,<sup>[a]</sup> Ruikuan Xie,<sup>[a]</sup> Qi Yin,<sup>[a]</sup> Meng-Di Zhang,<sup>[a]</sup> Qiao Wu,<sup>[a]</sup> Guo-Liang Chai,<sup>[a,b]</sup> Yuan-Biao Huang,<sup>✉[a,b]</sup> and Rong Cao<sup>✉[a,b]</sup>

- [a] Dr. J. Yi, Dr. D. Si, Dr. R. Xie, Dr. Q. Yin, M. Zhang, Q. Wu, Prof. G. Chai, Prof. Y. Huang, Prof. R. Cao  
State Key Laboratory of Structural Chemistry  
Fujian Institute of Research on the Structure of Matter, Chinese Academy of Sciences  
Fuzhou, 350002 (China)  
E-mail: ybhuang@fjirsm.ac.cn; rcao@fjirsm.ac.cn
- [b] Prof. G. Chai, Prof. Y. Huang, Prof. R. Cao  
University of Chinese Academy of Science  
Beijing 100049 (China)

Supporting information for this article is given via a link at the end of the document.

**Abstract:** The electrocatalytic conversion of CO<sub>2</sub> into value-added chemicals using renewable electricity is a promising approach to reduce atmospheric CO<sub>2</sub> concentration and realize carbon-energy balance. However, the low current density still limits CO<sub>2</sub> electroreduction reaction (CO<sub>2</sub>RR) for commercial application. Crystalline porous metal-organic frameworks (MOFs) are one class of promising alternatives for CO<sub>2</sub>RR due to their high CO<sub>2</sub> adsorption uptakes and periodically arranged isolated metal active sites. However, the poor conductivity and slow electron-transfer capability of the traditional MOFs usually result in low current density in CO<sub>2</sub>RR. Herein, conductive two-dimensional (2D) phthalocyanine-based MOF (NiPc-NiO<sub>4</sub>) nanosheets were prepared by the construction of nickel phthalocyanin-2,3,9,10,16,17,23,24-octaol (NiPc-OH) and nickel(II) ions, which can be employed as highly efficient electrocatalysts for CO<sub>2</sub>RR towards production of CO. The obtained NiPc-NiO<sub>4</sub> has a good conductivity with a high value of  $4.8 \times 10^{-5} \text{ S m}^{-1}$  due to the in-plane full  $\pi$ -d conjugation. Thus, the as-prepared NiPc-NiO<sub>4</sub> nanosheets exhibited a very high selectivity of 98.4% towards production of CO and a large CO partial current density of  $34.5 \text{ mA cm}^{-2}$ , outperforming the reported MOF catalysts. This work offers an opportunity to design conductive crystalline frameworks for improving energy efficiency in electrocatalysis.

## Introduction

Conversion of CO<sub>2</sub> to value-added chemicals could help reduce the atmospheric CO<sub>2</sub> concentration and alleviate the dependence on fossil fuels. Using electricity generated from renewable energy sources, CO<sub>2</sub> can be electrochemically reduced to energy-rich products such as carbon monoxide (CO), which is one of the most important feedstock to be used in the Fischer-Tropsch industrial process.<sup>[1-5]</sup> Over the past decades, various electrode materials for the conversion of CO<sub>2</sub>-to-CO have been explored, such as Au, Ag, Cu metals,<sup>[6-9]</sup> metal complexes<sup>[10-13]</sup> and single-atom Fe, Co, Ni based catalysts,<sup>[14-30]</sup>

metal-free carbons.<sup>[31-33]</sup> Nevertheless, it still remains several challenges for the CO<sub>2</sub> electroreduction reaction (CO<sub>2</sub>RR), including low energy conversion efficiency, poor selectivity and stability. Therefore, it still needs design and fabrication of highly active, selective and robust electrocatalysts towards CO<sub>2</sub>RR. Compared with Au, Ag, Cu-based inorganic solid catalysts, the tunable homogeneous molecular catalysts usually show enhanced selectivity and specific activity in CO<sub>2</sub>RR.<sup>[34]</sup> However, the extensive challenge for discrete metal complexes-based electrocatalysts is to achieve high selectivity and large current density in an aqueous medium. Loading electroactive metal complexes into porous conductive substrates is a promising approach to reduce CO<sub>2</sub> with high current density because of their fast electron transfer capacity and accessible active sites. Compared with other substrates, crystalline porous metal-organic frameworks (MOFs) with designable metal clusters and functional organic linkers have shown high selectivity in electrocatalytic CO<sub>2</sub>RR and other electrocatalytic reaction due to their single active sites and large CO<sub>2</sub> adsorption uptake.<sup>[35-51]</sup> However, the poor electrical conductivity feature of the traditionally insulating MOFs usually results in low current density in CO<sub>2</sub>RR. Hence, developing conductive MOFs (CMOFs) with highly single-active sites for CO<sub>2</sub>RR is extremely desirable.

As we know, metalphthalocyanine complexes with M-N<sub>4</sub> (e.g. M = Ni, Fe, Co) structures have been considered as typical active sites for CO<sub>2</sub>RR, but the selectivity and current density still need to be improved.<sup>[52-54]</sup> To address these problems, herein, Ni-phthalocyanine motif (NiPc) was integrated into a porous intrinsically conductive nickel-catecholate-linked two-dimensional (2D) MOF nanosheets (NiPc-NiO<sub>4</sub>, **Figure 1**) for the highly efficient CO<sub>2</sub>RR towards production of CO in aqueous medium. Notably, different from the traditional carboxylate-based MOFs, the CMOF NiPc-NiO<sub>4</sub>, in which the planar NiPc architecture was bridged by the nickel-catecholates, has good electrical conductivity because of the high d- $\pi$  orbital overlap between the nickel node and the catechol. Thus, the

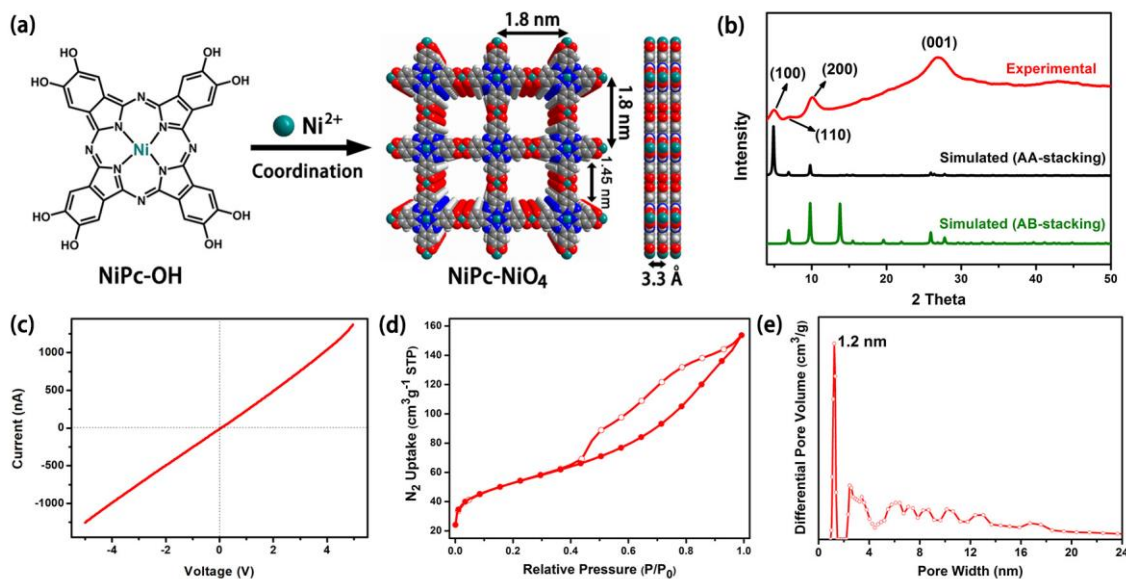


**Figure 1.** (a) Schematic illustration of the preparation of NiPc-NiO<sub>4</sub>. Top and side view of their structures with 2 × 2 square grids in AA-stacking mode. (b) Experimental PXRD patterns for NiPc-NiO<sub>4</sub> and simulated patterns with AA-packing and AB-stacking modes. (c) Current-voltage characteristic of NiPc-NiO<sub>4</sub> using two-contact probe method. (d) N<sub>2</sub> adsorption–desorption isotherms and (e) the pore size distribution (PSD) profile of NiPc-NiO<sub>4</sub>.

as-prepared NiPc-NiO<sub>4</sub> nanosheets exhibit outstanding electrocatalytic performance of CO<sub>2</sub>RR for production CO with nearly 100% selectivity (98.4 %) and a partial current density of 34.5 mA cm<sup>-2</sup> at -1.2 V versus the reversible hydrogen electrode (vs. RHE). The turnover frequency (TOF) can reach to 2603 h<sup>-1</sup> at -1.2 V vs. RHE and it also exhibits excellent long-term stability with 86% CO selectivity maintained after 10 hours chronoamperometry test. Moreover, the density functional theory calculation proves that the nickel of phthalocyanine center is the active site and NiPc-NiO<sub>4</sub> performs better activity than NiPc-OH due to the fast electron transfer capacity and excellent reducibility, which is consistent with the experiment results.

## Results and Discussion

The conjugated 2D CMOF NiPc-NiO<sub>4</sub> was synthesized by reaction of nickel phthalocyanine-2,3,9,10,16,17,23,24-octaol (NiPc-OH) and Ni(OAc)<sub>2</sub>·4H<sub>2</sub>O in water at 85 °C for 24 h (Figure 1a).<sup>[55]</sup> The powder X-ray diffraction (PXRD) pattern of the as-prepared NiPc-NiO<sub>4</sub> is well consistent with the AA-stacking model of the simulated one (Figure 1b), instead of AB-stacking model (Figure S1), suggesting the successful preparation of the crystalline NiPc-NiO<sub>4</sub>. The peaks at 5.2°, 7.0°, 10.1°, and 27.0° are assigned to (100), (110), (200), and (001) facets, respectively. Among them, the (001) facets at 27.0° indicated that NiPc-NiO<sub>4</sub> possess a square-shaped channel of 14.5 Å in diameter along the *c*-axis (Figure 1a-b). The layered phthalocyanine-based MOF features good carrier transport ability based on the large delocalized π system originating from the macrocyclic phthalocyanine structure itself and the dπ-pπ interaction between the nickel node and the catechol in these square-planar moieties. As expected, the electrical conductivity of NiPc-NiO<sub>4</sub> has a high value of 4.8 × 10<sup>-5</sup> S m<sup>-1</sup> measured at room temperature using a two-contact probe method (Figure 1c).<sup>[56]</sup> Such good electrical conductivity would be beneficial for the electron transfer to the active sites during CO<sub>2</sub>RR, thereby improving energy conversion efficiency and electrochemical

activity. The N<sub>2</sub> sorption measurement at 77 K revealed that the 2D NiPc-NiO<sub>4</sub> has a high Brunauer-Emmett-Teller (BET) surface area of 180 cm<sup>3</sup> g<sup>-1</sup> (Figure 1d). The pore size distribution analysis (Figure 1e) indicated that NiPc-NiO<sub>4</sub> possesses micropore of 1.2 nm, which is consistent with the theoretical size of the square shaped channels along the *c* direction (Figure 1a). Moreover, many mesopores ranging from 2 nm to 18 nm were formed in NiPc-NiO<sub>4</sub>, which may be originated from the stacking gaps and defects between microcrystalline particles. Besides, NiPc-NiO<sub>4</sub> shows a high CO<sub>2</sub> adsorption uptake of 16.8 cm<sup>3</sup> g<sup>-1</sup>

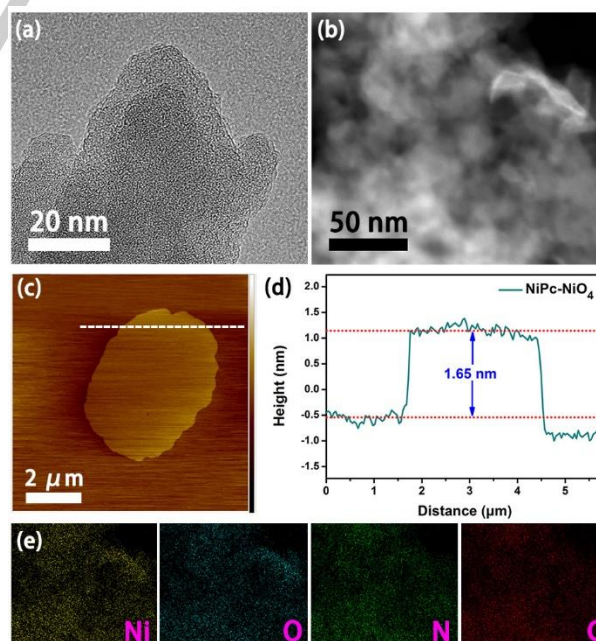


**Figure 2.** (a) TEM image and (b) HAADF-STEM image of NiPc-NiO<sub>4</sub>. (c) AFM image of NiPc-NiO<sub>4</sub>. (d) The height profile along the white line in (c). (e) The elemental mapping of Ni, O, N, and C for NiPc-NiO<sub>4</sub>.

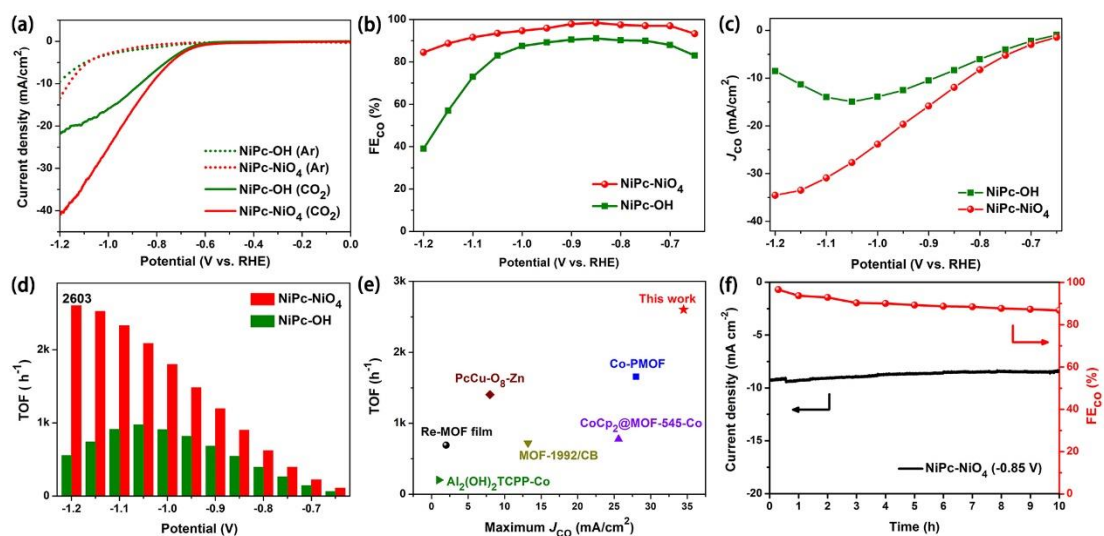


**Figure 3.** (a) LSV curves of NiPc-NiO<sub>4</sub> and NiPc-OH in CO<sub>2</sub>, and Ar-saturated 0.5 M KHCO<sub>3</sub>. (b) Faradaic efficiencies of CO. (c) CO partial current density, (d) turnover frequency for NiPc-NiO<sub>4</sub> and NiPc-OH. (e) Comparison of the TOF and maximum CO partial current density with reported MOF catalysts, including Co-PMOF,<sup>[29]</sup> CoCp<sub>2</sub>@MOF-545-Co,<sup>[30]</sup> PcCu-O<sub>8</sub>-Zn,<sup>[31]</sup> MOF-1992/CB,<sup>[32]</sup> Re-MOF film,<sup>[33]</sup> Al<sub>2</sub>(OH)<sub>2</sub>TCPP-Co.<sup>[34]</sup> (f) Stability of NiPc-NiO<sub>4</sub> at a potential of -0.85 V versus RHE for 10 h.

at room temperature (Figure S2), which would facilitate in promoting CO<sub>2</sub>RR.

The morphology of the as-prepared NiPc-NiO<sub>4</sub> was characterized by scanning electron microscopy (SEM) and transmission electron microscopy (TEM). The SEM images in Figure S3 show that the obtained NiPc-NiO<sub>4</sub> was composed of nanoparticles (NPs) of less than 100 nm. The TEM (Figure 2a) and high angle annular dark-field scanning transmission electron microscopy (HAADF-STEM) images (Figure 2b) display no aggregated Ni NPs. To ensure the accessible of the Ni active sites in the slipped AA stacking frameworks for the electrolytes and CO<sub>2</sub>, the ultrathin 2D NiPc-NiO<sub>4</sub> nanosheets were successfully fabricated by exfoliating from its bulk via high-frequency sonication at room temperature. As shown the atomic force microscopy (AFM) image and its height profile in Figure 2c-2d, a uniform thickness of ca. 1.65 nm was clearly observed, which is close to five layers of NiPc-NiO<sub>4</sub> nanosheets. Such ultrathin 2D NiPc-NiO<sub>4</sub> nanosheets would facilitate in exposure of more the Ni active sites for the CO<sub>2</sub> and electrolytes, thus improving CO<sub>2</sub>RR activity. Furthermore, the corresponding element mapping analysis of NiPc-NiO<sub>4</sub> indicated Ni, N, O and C elements were homogeneously distributed over the entire structure (Figure 2e). The results indicated that the Ni species in NiPc-NiO<sub>4</sub> are positioned in isolated sites.

To examine the catalytic performance of the as-prepared NiPc-NiO<sub>4</sub> nanosheets towards CO<sub>2</sub>RR in 0.5 M KHCO<sub>3</sub> solution, a conductive ink containing NiPc-NiO<sub>4</sub> was prepared and drop-casted on carbon paper electrode. The catalytic activity was evaluated in a three-electrode system using a two-compartment H-type cell that separated by a proton-exchange membrane. All the potentials mentioned in this work are with reference to the reversible hydrogen electrode (RHE). As shown in Figure 3a, the onset potentials of both NiPc-OH and NiPc-NiO<sub>4</sub> in CO<sub>2</sub> atmosphere are more positive than that of in Ar atmosphere, indicating that their activities are originated from the CO<sub>2</sub>RR. Furthermore, as shown in Figure 3b, NiPc-NiO<sub>4</sub> nanosheets show high Faradaic efficiencies of CO with above 90% in a wide

potential range from -0.65 V to -1.1 V, reaching the maximum of 98.4% at -0.85 V, surpassing most of reported MOF catalysts (Table S1).<sup>[35-48]</sup> Moreover, the CO partial current density of NiPc-NiO<sub>4</sub> gradually increases with the increase of the overpotential, reaching 34.5 mA cm<sup>-2</sup> at -1.2 V (Figure 3c), which is the largest value among the reported MOFs (Table S1) and about 4 times of that NiPc-OH monomer (Figure S4). The excellent electrocatalytic CO<sub>2</sub>RR performance for NiPc-NiO<sub>4</sub> nanosheets highlights the importance of their good electrical conductivity, accessible single active sites, and large CO<sub>2</sub> adsorption capacity.

In order to determine whether the catalytically active site is the nickel of phthalocyanine center or NiO<sub>4</sub> node, the typical 2D CMOF Ni<sub>3</sub>(HHTP)<sub>2</sub> containing only NiO<sub>4</sub> node was synthesized for CO<sub>2</sub>RR under the same conditions.<sup>[57]</sup> As shown in Figure S5, the main product of Ni<sub>3</sub>(HHTP)<sub>2</sub> is H<sub>2</sub> with selectivity of around 95% throughout the testing range of -0.7 to -1.2 V, indicating that the NiO<sub>4</sub> node cannot catalyze the CO<sub>2</sub>RR and can be excluded as the active site in NiPc-NiO<sub>4</sub> for CO<sub>2</sub>RR. Besides, pure ketjen black and carbon paper electrode also only produce H<sub>2</sub> (Figure S6 and S7), while the ligand NiPc-OH shows certain CO<sub>2</sub>RR activity, indicating that the active site in NiPc-NiO<sub>4</sub> is the Ni<sub>4</sub> sites of NiPc moiety. Thus, on the basis of the NiPc motif as active site, the turnover frequency (TOF) of the NiPc-NiO<sub>4</sub> was calculated and summarized in Figure 3d. The TOF of NiPc-NiO<sub>4</sub> gradually increases with the increasing overpotential, reaching a maximum of 2603 h<sup>-1</sup> at -1.2 V. To the best of our knowledge, such high TOF and CO partial current density are better than any state-of-the-art MOF catalysts (Figure 3e). The long-term stability is another important factor for evaluating the practicability of catalysts. As shown in Figure 3f, after 10 hours durability test at -0.85 V, the current density of NiPc-NiO<sub>4</sub> did not change significantly by decreasing only 0.8 mA cm<sup>-2</sup>, while the high CO selectivity of 86% for NiPc-NiO<sub>4</sub> was still maintained. The result indicates the superior structural stability of NiPc-NiO<sub>4</sub> in this neutral aqueous medium. Moreover, no Ni NPs were observed in the TEM images of the NiPc-NiO<sub>4</sub> after

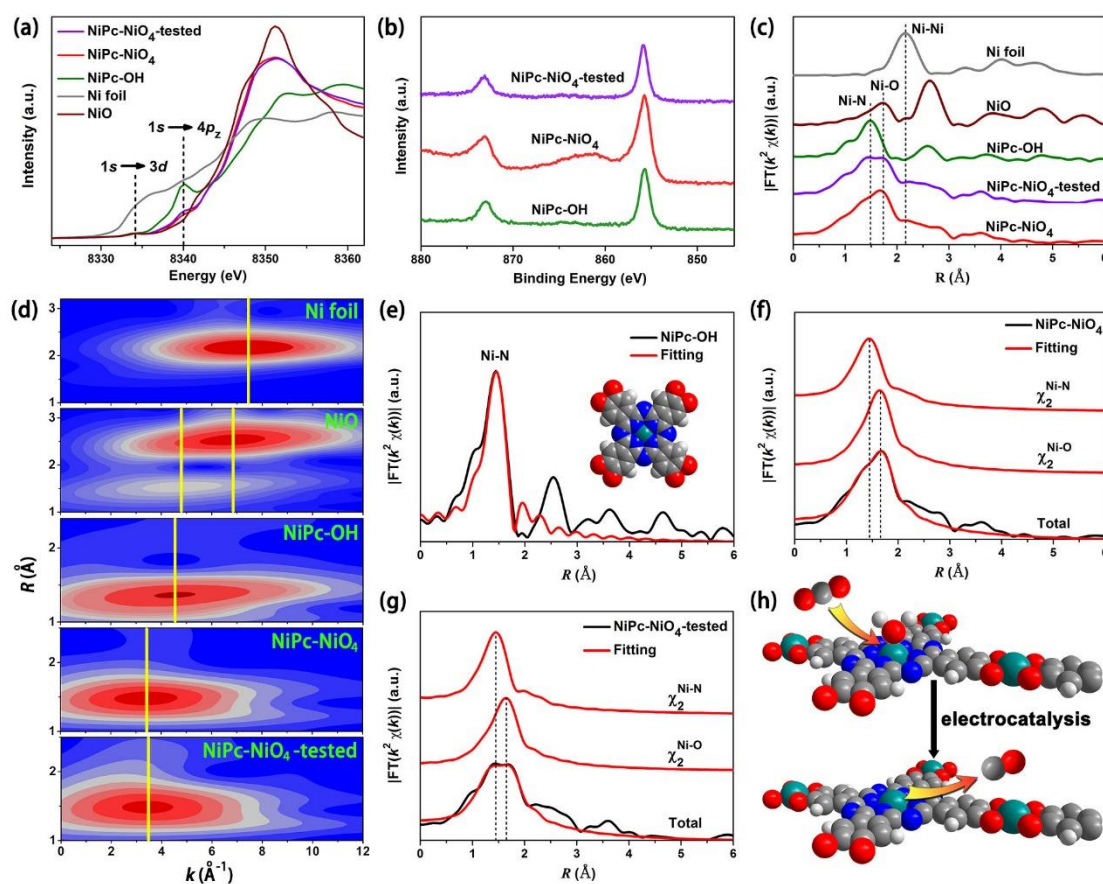


**Figure 4.** (a) Normalized Ni  $K$ -edge XANES spectra of Ni foil, NiO, NiPc-OH, NiPc-NiO<sub>4</sub> and NiPc-NiO<sub>4</sub>-tested. (b) XPS spectra of the Ni 2p region of NiPc-OH, NiPc-NiO<sub>4</sub> and NiPc-NiO<sub>4</sub>-tested. (c) Fourier transform EXAFS spectra of different samples. (d) Wavelet transforms for the  $k^2$ -weighted EXAFS signals of different samples. The corresponding EXAFS fitting curves of (e) NiPc-OH, (f) NiPc-NiO<sub>4</sub> (g) NiPc-NiO<sub>4</sub>-tested. The inset in (e) is the molecule architecture of NiPc-OH. (h) Schematic illustration of the transformation process throughout the CO<sub>2</sub>RR reaction.

electrocatalysis (Figure S9-S10), and the post-reaction SEM images showed no significant changes in the size and shape (Figure S11), suggesting that no structural collapse of NiPc-NiO<sub>4</sub> was occurred and no crystalline metal impurities generated during the CO<sub>2</sub>RR process. Furthermore, the major peaks were remained in the PXRD of NiPc-NiO<sub>4</sub> after the CO<sub>2</sub>RR measurement (NiPc-NiO<sub>4</sub>-tested) (Figure S12), indicating that the crystalline framework of NiPc-NiO<sub>4</sub> was still maintained in this neutral electrochemical testing system. To further determine whether CO was produced from the CO<sub>2</sub>RR, the <sup>13</sup>C-labeling CO<sub>2</sub> isotope experiments were conducted via gas chromatography-mass spectrometry (GC-MS). As shown in Figure S13, when conducting CO<sub>2</sub>RR with <sup>13</sup>C-labeling CO<sub>2</sub> in 0.5 M KH<sup>12</sup>CO<sub>3</sub>, both the signal of <sup>12</sup>CO and <sup>13</sup>CO was observed, while only <sup>13</sup>CO was observed in KCl electrolyte. These results demonstrate that CO was originated from the CO<sub>2</sub> in equilibrium with bicarbonate anions in CO<sub>2</sub>-saturated KHCO<sub>3</sub> aqueous solution.<sup>[58-60]</sup>

In order to further figure out the coordination environment and electronic structure of Ni active sites during the CO<sub>2</sub>RR, the *ex situ* synchrotron based X-ray absorption spectroscopy (XAS) and X-ray photoelectron spectroscopy (XPS) were carried out. The X-ray absorption near edge structure (XANES) of Ni  $K$  edge in Figure 4a shows that the XANES curves of NiPc-NiO<sub>4</sub> and

NiPc-NiO<sub>4</sub>-tested almost overlap together, indicating that the structure of NiPc-NiO<sub>4</sub> maintained well after the CO<sub>2</sub>RR process. In addition, two fingerprint peaks of NiN<sub>4</sub> symmetrical structure were found at 8334 eV and 8340 eV in NiPc-OH, NiPc-NiO<sub>4</sub> and NiPc-NiO<sub>4</sub>-tested. One at 8334 eV is assignable to the dipole forbidden 1s to 3d transition, and the other one at 8340 eV is attributed to the shaken-down satellite 1s to 4p<sub>z</sub> transition.<sup>[61-62]</sup> The presence of these two NiN<sub>4</sub> fingerprint peaks in NiPc-NiO<sub>4</sub>-tested reveals that the nickel atom in the center of phthalocyanine maintains the NiN<sub>4</sub> structure after CO<sub>2</sub>RR, instead of detaching from the phthalocyanine center and aggregating together. Both of the white line positions of NiPc-NiO<sub>4</sub> and NiPc-NiO<sub>4</sub>-tested are very close to that of NiO, indicating that the valence state of the Ni atoms in these samples is close to +2.<sup>[61-62]</sup> The XPS results also indicated the dominance of Ni<sup>2+</sup> in all the samples, consistent with the XANES analysis. As shown in Figure 4b, the Ni 2p XPS spectra of the three samples display the similar patterns with two peaks at 873.0 eV and 855.7 eV, which can be assigned to Ni 2p<sub>1/2</sub> and Ni 2p<sub>3/2</sub>, respectively.<sup>[61-63]</sup> What's more, cyclic voltammetry (CV) measurement could be used to analyze the dynamic change process of oxidation state. As shown in Figure S14, the CV curves of NiPc-NiO<sub>4</sub> were conducted in an anhydrous system (0.1 M TBAPF<sub>6</sub>/acetonitrile) in order to eliminate the effect of the

redox peaks of water. There is a pair of redox peaks assigned to the conversion between Ni(II) and Ni(I) in the CV tested in argon atmosphere, while no obvious redox peaks are observed in CO<sub>2</sub> atmosphere, which may be due to the electrons are quickly transferred from the formed Ni(I) species to the CO<sub>2</sub> substrate molecules. According to the CV results, it is suggested that Ni(II) could be reduced to Ni(I) under cathodic bias during CO<sub>2</sub>RR, which would be quickly oxidized back to Ni(II) after the electrons transferred from the formed Ni(I) species to the CO<sub>2</sub> substrate molecules.<sup>[64]</sup>

The coordination environment of the nickel atoms in the samples are further analyzed by extended X-ray absorption fine structure (EXAFS). As shown in **Figure 4c**, compared with Ni foil sample, no Ni-Ni bond at 2.2 Å was observed in NiPc-OH, NiPc-NiO<sub>4</sub> and NiPc-NiO<sub>4</sub>-tested, indicating that all the nickel atoms in these samples exist as single Ni site without the presence of metal-derived aggregates. The results revealed that the NiPc sites and NiO<sub>4</sub> nodes in NiPc-NiO<sub>4</sub> were not reduced to NPs during CO<sub>2</sub>RR process. Besides, the NiPc-OH, NiPc-NiO<sub>4</sub> and NiPc-NiO<sub>4</sub>-tested samples have one main peak at 1.4 Å that attributed to the Ni-N bond, while the latter two samples show another peak centered at 1.6 Å, which overlaps with the Ni-O bond in NiO and can therefore be attributed to the NiO<sub>4</sub> node.<sup>[65]</sup> These results indicated that the NiPc sites and NiO<sub>4</sub> nodes in NiPc-NiO<sub>4</sub> were well maintained after CO<sub>2</sub>RR.

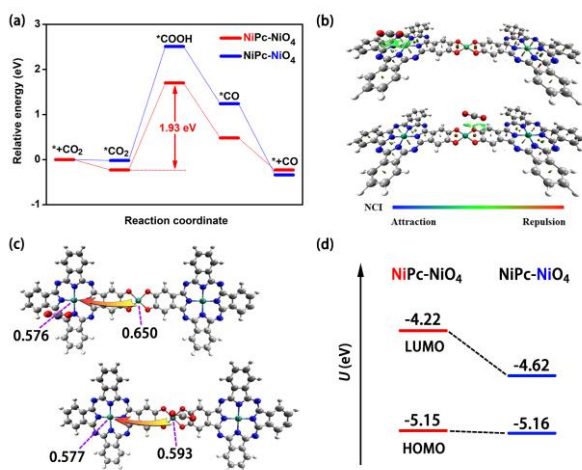


**Figure 5.** (a) Calculated energy diagrams for CO<sub>2</sub>-to-CO conversion on two proposed active sites in NiPc-NiO<sub>4</sub>. (b) The noncovalent interaction (NCI) between CO<sub>2</sub> and NiPc-NiO<sub>4</sub> structure. (c) The Mulliken charge of different Ni atoms in NiPc-NiO<sub>4</sub>. (d) The energy level of HOMO and LUMO of different Ni atoms in NiPc-NiO<sub>4</sub> with introduction of CO<sub>2</sub>.

EXAFS wavelet transform (WT) analysis is powerful for discriminating the backscattering atoms in *R*-space, by providing radial distance resolution and *k*-space resolution.<sup>[65-67]</sup> In the EXAFS WT contour plots of Ni foil (**Figure 4d**), only one intensity maximum at 7.4 Å<sup>-1</sup> ascribed to the Ni-Ni bond was observed. While two intensity maximum at 4.8 and 6.9 Å<sup>-1</sup> were observed in NiO standard sample, which can be ascribed to the Ni-O and Ni-Ni bond, respectively. Notably, only one intensity maximum at 3.4 Å<sup>-1</sup> ascribed to the Ni-N(O) bonding was observed and no intensity maximum corresponded to Ni-Ni bonding existed in NiPc-NiO<sub>4</sub> and NiPc-NiO<sub>4</sub>-tested, further demonstrating that the nickel species were presented with

isolated atomic-level dispersion. To obtain quantitative structural parameters of the Ni atoms, a least-squares EXAFS fitting was carried out and the fitting results are shown in **Figure 4e-4g**, **Figure S15-S16** and **Table S2**. The fitting result of NiPc-NiO<sub>4</sub> indicated that the average coordination number of Ni-N and Ni-O bond are 4.0 and 5.5, respectively. The larger coordination number of Ni-O bond in comparison with the theoretical value can be reasonably ascribed to the axial coordinated H<sub>2</sub>O molecules adsorbed on NiO<sub>4</sub> nodes. In general, the analysis of the oxidation states and the precise coordination environment of Ni atoms throughout the CO<sub>2</sub>RR process demonstrate the superior structure stability of NiPc-NiO<sub>4</sub> and the full exposure of active sites.

To further determine whether the catalytically active site is the nickel of phthalocyanine center (NiPC) or NiO<sub>4</sub> node, we calculated the energy for CO<sub>2</sub>RR and hydrogen evolution reaction (HER) at two different Ni active sites in NiPc-NiO<sub>4</sub> (**Table S3**). For the NiPC, the energies of the rate-determining step (RDS) for CO<sub>2</sub>RR (formation of COOH\* intermediate) and HER (formation of H\*) are 1.93 eV (**Figure 5a**) and 1.98 eV (**Figure S17**), respectively, suggesting that CO<sub>2</sub>RR occurs preferentially at NiPC sites. In contrast, the corresponding energy for CO<sub>2</sub>RR (2.53 eV, **Figure 5a**) in the nickel of the NiO<sub>4</sub> node is larger than that of HER (1.58 eV, **Figure S17**), which indicated that HER takes precedence at NiO<sub>4</sub> nodes. Moreover, the energy for RDS on the NiPC (1.93 eV) is significantly lower than that on NiO<sub>4</sub> node (2.53 eV), which clearly shows that NiPC is the active site for CO<sub>2</sub>RR. The above calculated results are in agreement with the experiment results that NiPc-OH showed active for CO<sub>2</sub>RR (**Figure 3b**) while Ni<sub>3</sub>(HHTP)<sub>2</sub> exhibited only catalytic HER performance (**Figure S5**).

The high activity and selectivity of NiPC in the CO<sub>2</sub>RR can be further explained in terms of adsorption capacity, charge distribution, and reducibility. Firstly, the adsorption energies of CO<sub>2</sub> on NiPC and NiO<sub>4</sub> node are 0.23 eV and 0.02 eV (**Table S3**), respectively. Thus, the CO<sub>2</sub> molecular was easier to combine with NiPC, which is also revealed by noncovalent-interaction. As shown in **Figure 5b**, there is stronger Van der Waals interaction between CO<sub>2</sub> molecule and NiPC than that of NiO<sub>4</sub> node. Secondly, the Mulliken population analysis of the two Ni atoms indicates the more electron-rich environment of NiPC compared with Ni in NiO<sub>4</sub> node, no matter that whether Ni atom was or not adsorbed by CO<sub>2</sub> molecule (**Figure 5c**). Thirdly, the lowest unoccupied molecular orbital (LUMO) energy level of NiPc-NiO<sub>4</sub> shifts from -4.22 eV to -4.62 eV when the CO<sub>2</sub> molecule moves from NiPC to NiO<sub>4</sub> node (**Figure 5d**), indicating the excellent reducibility of NiPC. Thus, the Ni of phthalocyanine center is an excellent active site on account of its strong adsorption capacity of CO<sub>2</sub>, electron-rich environment and excellent reducibility.

We also calculated the energy required for CO<sub>2</sub>RR of NiPc molecule. As shown in **Figure S18**, the energy for RDS towards CO<sub>2</sub>RR by NiPc molecule is 3.12 eV, which is quite larger than that of the Ni of phthalocyanine center (1.93 eV) in NiPc-NiO<sub>4</sub>. The result indicated that the catalytic capacity of the Ni active site has been significantly improved after the phthalocyanine molecules are inserted into the 2D conductive MOF material. This improvement can be reasonably ascribed to the dπ-pπ interaction between the nickel node and the catechol in the square-planar NiPc-NiO<sub>4</sub>.

## Conclusion

In summary, nickel phthalocyanine molecules as active sites were installed into nickel-catecholate-linked 2D conductive metal-organic framework (NiPc-NiO<sub>4</sub>) nanosheets for efficiently CO<sub>2</sub> electroreduction reaction. Due to the in-plane full  $\pi$ -d conjugation between the phthalocyanine molecule and the NiO<sub>4</sub> nodes, NiPc-NiO<sub>4</sub> has good conductivity of  $4.8 \times 10^{-5} \text{ S m}^{-1}$ . Hence, the as-prepared 2D NiPc-NiO<sub>4</sub> nanosheets show outstanding activity towards CO<sub>2</sub> electroreduction with nearly 100% CO selectivity, large CO partial current density up to 34.5 mA cm<sup>-2</sup>, high turnover frequency up to 2603 h<sup>-1</sup>, and excellent long-term durability. To the best of our knowledge, such high TOF and CO partial current density is better than any state-of-the-art MOF catalysts. The density functional theory calculation proves that the nickel of phthalocyanine center is the active sites and NiPc-NiO<sub>4</sub> performs better activity than the phthalocyanine molecules due to the fast electron transfer capacity and excellent reducibility, which is consistent with the experiment results. Our work provides an effective strategy to improve the CO<sub>2</sub> electroreduction performance by designing conductive crystalline frameworks with uniformly distributed phthalocyanine active sites. It also builds a bridge between the homogeneous molecule catalysts and heterogeneous porous catalysts.

## Acknowledgements

We acknowledge the financial support from the National Key Research and Development Program of China (2018YFA0208600, 2018YFA0704502), NSFC (21871263, 22071245, 21671188, 22033008), Strategic Priority Research Program of the Chinese Academy of Sciences (XDB20000000), Youth Innovation Promotion Association, CAS (Y201850). We thank the beamline BL14W1 station for XAS measurements at the Shanghai Synchrotron Radiation Facility, China. We thank Prof. Xu Gang for the assistance of the conductivity measurements.

## Conflict of interest

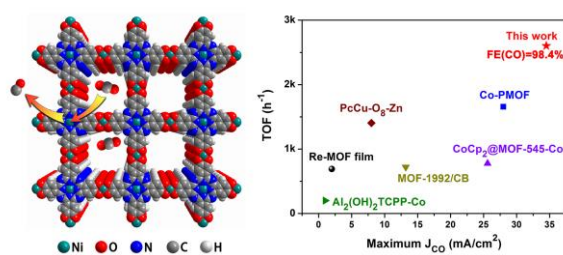
The authors declare no conflict of interest.

**Keywords:** Conductive metal-organic framework • CO<sub>2</sub> electroreduction • CO • phthalocyanine

- [1] D. Gao, R. M. Arán-Ais, H. S. Jeon, B. Roldan Cuenya, *Nat. Catal.* **2019**, *2*, 198–210.
- [2] C. Long, X. Li, J. Guo, Y. Shi, S. Liu, Z. Tang, *Small Methods* **2018**, *1800369*.
- [3] W. Zhang, Y. Hu, L. Ma, G. Zhu, Y. Wang, X. Xue, R. Chen, S. Yang, Z. Jin, *Adv. Sci.* **2018**, *5*, 1700275.
- [4] H. Yang, X. Wang, Q. Hu, X. Chai, X. Ren, Q. Zhang, J. Liu, C. He, *Small Methods* **2020**, *4*, 1900826.
- [5] Y. Wang, P. Han, X. Lv, L. Zhang, G. Zheng, *Joule* **2018**, *2*, 2551–2582.
- [6] M. Liu, Y. Pang, B. Zhang, P. De Luna, O. Voznyy, J. Xu, X. Zheng, C. T. Dinh, F. Fan, C. Cao, F. P. G. De Arquer, T. S. Safaei, A. Mepham, A. Klinkova, E. Kumacheva, T. Filleter, D. Sinton, S. O. Kelley, E. H. Sargent, *Nature* **2016**, *537*, 382–386.
- [7] F. P. G. De Arquer, C. Dinh, A. Ozden, J. Wicks, C. Mccallum, A. R. Kirmani, D. Nam, C. Gabardo, A. Seifitokaldani, X. Wang, Y. C. Li, F. Li, J. Edwards, L. J. Richter, S. J. Thorpe, D. Sinton, E. H. Sargent, *Science* **2020**, *367*, 661–666.
- [8] C. Zhao, G. Luo, X. Liu, W. Zhang, Z. Li, Q. Xu, Q. Zhang, H. Wang, D. Li, F. Zhou, Y. Qu, X. Han, Z. Zhu, G. Wu, J. Wang, J. Zhu, T. Yao, Y. Li, H. J. M. Bouwmeester, Y. Wu, *Adv. Mater.* **2020**, *32*, 2002382.
- [9] J. Yang, X. Wang, Y. Qu, X. Wang, H. Huo, Q. Fan, J. Wang, L. M. Yang, Y. Wu, *Adv. Energy Mater.* **2020**, *10*, 2001709.
- [10] X. Sun, L. Lu, Q. Zhu, C. Wu, D. Yang, C. Chen, B. Han, *Angew. Chem. Int. Ed.* **2018**, *57*, 2427–2431.
- [11] Y. Peng, L. Wang, Q. Luo, Y. Cao, Y. Dai, Z. Li, H. Li, X. Zheng, W. Yan, J. Yang, J. Zeng, *Chem* **2018**, *4*, 613–625.
- [12] F. Li, L. Chen, G. P. Knowles, D. R. Macfarlane, J. Zhang, *Angew. Chem. Int. Ed.* **2017**, *56*, 505–509.
- [13] D. Yang, Q. Zhu, X. Sun, C. Chen, W. Guo, G. Yang, B. Han, *Angew. Chem. Int. Ed.* **2020**, *59*, 2354–2359.
- [14] H. J. Zhu, M. Lu, Y. R. Wang, S. J. Yao, M. Zhang, Y. H. Kan, J. Liu, Y. Chen, S. L. Li, Y. Q. Lan, *Nat. Commun.* **2020**, *11*, 497.
- [15] Y. Hou, Y. B. Huang, Y. L. Liang, G. L. Chai, J. D. Yi, T. Zhang, K. T. Zang, J. Luo, R. Xu, H. Lin, S. Y. Zhang, H. M. Wang, R. Cao, *CCS Chem.* **2019**, *1*, 384–395.
- [16] H. Yang, Y. Wu, G. Li, Q. Lin, Q. Hu, Q. Zhang, J. Liu, C. He, *J. Am. Chem. Soc.* **2019**, *141*, 12717–12723.
- [17] Q. Wu, R. K. Xie, M. J. Mao, G. L. Chai, J. D. Yi, S. S. Zhao, Y. B. Huang, R. Cao, *ACS Energy Lett.* **2020**, *5*, 1005–1012.
- [18] A. Guan, Z. Chen, Y. Quan, C. Peng, Z. Wang, T. Sham, C. Yang, Y. Ji, L. Qian, X. Xu, G. Zheng, *ACS Energy Lett.* **2020**, *5*, 1044–1053.
- [19] J. Gu, C. S. Hsu, L. Bai, H. M. Chen, X. Hu, *Science* **2019**, *364*, 1091–1094.
- [20] M. D. Zhang, D. H. Si, J. D. Yi, S. S. Zhao, Y. B. Huang, R. Cao, *Small* **2020**, *16*, 2005254.
- [21] J. Yang, Z. Qiu, C. Zhao, W. Wei, W. Chen, Z. Li, Y. Qu, J. Dong, J. Luo, Z. Li, Y. Wu, *Angew. Chem. Int. Ed.* **2018**, *57*, 14095–14100.
- [22] C. Yan, H. Li, Y. Ye, H. Wu, F. Cai, R. Si, J. Xiao, S. Miao, S. Xie, F. Yang, Y. Li, G. Wang, X. Bao, *Energy Environ. Sci.* **2018**, *11*, 1204–1210.
- [23] Q. Wu, J. Liang, Z. L. Xie, Y. B. Huang, R. Cao, *ACS Materials Lett.* **2021**, *3*, 454–461.
- [24] X. Li, W. Bi, M. Chen, Y. Sun, H. Ju, W. Yan, J. Zhu, X. Wu, W. Chu, C. Wu, Y. Xie, *J. Am. Chem. Soc.* **2017**, *139*, 14889–14892.
- [25] C. Zhao, Y. Wang, Z. Li, W. Chen, Q. Xu, D. He, D. Xi, Q. Zhang, T. Yuan, Y. Qu, J. Yang, F. Zhou, Z. Yang, X. Wang, J. Wang, J. Luo, Y. Li, H. Duan, Y. Wu, Y. Li, *Joule* **2019**, *3*, 584–594.
- [26] M. D. Zhang, D. H. Si, J. D. Yi, Q. Yin, Y. B. Huang, R. Cao, *Sci. China Chem.* DOI: 10.1007/s11426-021-1022-3.
- [27] H. Bin Yang, S. Hung, S. Liu, K. Yuan, S. Miao, L. Zhang, X. Huang, H. Wang, W. Cai, R. Chen, J. Gao, X. Yang, W. Chen, Y. Huang, H. M. Chen, C. M. Li, T. Zhang, B. Liu, *Nat. Energy* **2018**, *3*, 140–147.
- [28] C. Zhao, X. Dai, T. Yao, W. Chen, X. Wang, J. Wang, J. Yang, S. Wei, Y. Wu, Y. Li, *J. Am. Chem. Soc.* **2017**, *139*, 8078–8081.
- [29] Q. Wu, M. J. Mao, Q. J. Wu, J. Liang, Y. B. Huang, R. Cao, *Small* DOI: 10.1002/smll.202004933.
- [30] X. Wang, Z. Chen, X. Zhao, T. Yao, W. Chen, R. You, C. Zhao, G. Wu, J. Wang, W. Huang, J. Yang, X. Hong, S. Wei, Y. Wu, Y. Li, *Angew. Chem. Int. Ed.* **2018**, *57*, 1944–1948.
- [31] B. Pan, X. Zhu, Y. Wu, T. Liu, X. Bi, K. Feng, N. Han, J. Zhong, J. Lu, Y. Li, Y. Li, *Adv. Sci.* **2020**, *7*, 2001002.
- [32] J. Xie, X. Zhao, M. Wu, Q. Li, Y. Wang, J. Yao, *Angew. Chem. Int. Ed.* **2018**, *57*, 9640–9644.
- [33] Y. Wang, J. Chen, G. Wang, Y. Li, Z. Wen, *Angew. Chem. Int. Ed.* **2018**, *57*, 13120–13124.
- [34] L. Sun, V. Reddu, A. C. Fisher, X. Wang, *Energy Environ. Sci.* **2020**, *13*, 374–403.
- [35] Y. R. Wang, Q. Huang, C. T. He, Y. Chen, J. Liu, F. C. Shen, Y. Q. Lan, *Nat. Commun.* **2018**, *9*, 4466.
- [36] Z. Xin, Y. R. Wang, Y. Chen, W. L. Li, L. Z. Dong, Y. Q. Lan, *Nano Energy* **2020**, *67*, 104233.

- [37] H. Zhong, M. Ghorbani-asl, K. H. Ly, J. Zhang, J. Ge, M. Wang, Z. Liao, D. Makarov, E. Zschech, E. Brunner, I. M. Weidinger, J. Zhang, A. V. Krasheninnikov, S. Kaskel, R. Dong, X. Feng, *Nat. Commun.* **2020**, *11*, 1409.
- [38] R. Matheu, E. Gutierrez-Puebla, M. Á. Monge, C. S. Diercks, J. Kang, M. S. Prévot, X. Pei, N. Hanikel, B. Zhang, P. Yang, O. M. Yaghi, *J. Am. Chem. Soc.* **2019**, *141*, 17081–17085.
- [39] L. Ye, J. Liu, Y. Gao, C. Gong, M. Addicoat, T. Heine, C. Woll, L. Sun, *J. Mater. Chem. A* **2016**, *4*, 15320–15326.
- [40] N. Komienko, Y. Zhao, C. S. Kley, C. Zhu, D. Kim, S. Lin, C. J. Chang, O. M. Yaghi, P. Yang, *J. Am. Chem. Soc.* **2015**, *137*, 14129–14135.
- [41] F. Mao, Y.-H. Jin, P. Liu, P. Yang, L. Zhang, L. Chen, X.-M. Cao, J. Gu, H. Yang, *J. Mater. Chem. A* **2019**, *7*, 23055–23063.
- [42] Y. Guo, W. Shi, H. Yang, Q. He, Z. Zeng, J. Ye, X. He, R. Huang, C. Wang, W. Lin, *J. Am. Chem. Soc.* **2019**, *141*, 17875–17883.
- [43] B. Dong, S. Qian, F. Bu, Y. Wu, L.-G. Feng, Y.-L. Teng, W.-L. Liu, Z.-W. Li, *ACS Appl. Energy Mater.* **2018**, *1*, 4662–4669.
- [44] Z. Yang, X. Zhang, C. Long, S. Yan, Y. Shi, J. Han, J. Zhang, P. An, L. Chang, Z. Tang, *CrystEngComm* **2020**, *22*, 1619–1624.
- [45] S. Dou, J. Song, S. Xi, Y. Du, J. Wang, Z. Huang, Z. Xu, X. Wang, *Angew. Chem. Int. Ed.* **2019**, *58*, 4041–4045.
- [46] X. Jiang, H. Li, J. Xiao, R. Si, F. Yang, Y. Li, X. Bao, *Nano Energy* **2018**, *52*, 345–350.
- [47] Y. Wang, P. Hou, Z. Wang, P. Kang, *ChemPhysChem* **2017**, *18*, 3142–3147.
- [48] I. Hod, M. D. Sampson, P. Deria, C. P. Kubiak, O. K. Farha, J. T. Hupp, I. Hod, M. D. Sampson, P. Deria, C. P. Kubiak, O. K. Farha, T. Joseph, *ACS Catal.* **2015**, *5*, 6302–6309.
- [49] J. Su, W. He, X. M. Li, L. Sun, H. Y. Wang, Y. Q. Lan, M. Ding, J. L. Zuo, *Matter* **2020**, *2*, 711–722.
- [50] W. Xiong, H. Li, H. You, M. Cao, R. Cao, *Natl. Sci. Rev.* **2020**, *7*, 609–619.
- [51] J. D. Yi, R. K. Xie, Z. L. Xie, G. L. Chai, T. F. Liu, R. P. Chen, Y. B. Huang, R. Cao, *Angew. Chem. Int. Ed.* **2020**, *59*, 23641–23648.
- [52] Z. Zhang, J. Xiao, X. J. Chen, S. Yu, L. Yu, R. Si, Y. Wang, S. Wang, X. Meng, Y. Wang, Z. Q. Tian, D. Deng, *Angew. Chem. Int. Ed.* **2018**, *57*, 16339–16342.
- [53] M. Lu, M. Zhang, C. G. Liu, J. Liu, L. J. Shang, M. Wang, J. N. Chang, S. L. Li, Y. Q. Lan, *Angew. Chem. Int. Ed.* **2021**, *60*, 4864–4871.
- [54] L. Lin, T. Liu, J. Xiao, H. Li, P. Wei, D. Gao, B. Nan, R. Si, G. Wang, X. Bao, *Angew. Chem. Int. Ed.* **2020**, *59*, 22408–22413.
- [55] Z. Meng, A. Aykanat, K. A. Mirica, *J. Am. Chem. Soc.* **2019**, *141*, 2046–2053.
- [56] L. Sun, S. S. Park, D. Sheberla, M. Dincă, *J. Am. Chem. Soc.* **2016**, *138*, 14772–14782.
- [57] H. Furukawa, S. Wan, V. Augustyn, R. Chang, L. Liao, F. Zhou, E. Perre, V. Ozolins, K. Suenaga, X. Duan, B. Dunn, Y. Yamamoto, O. Terasaki, O. M. Yaghi, *Chem. Mater.* **2012**, *24*, 3511–3513.
- [58] M. Dunwell, Q. Lu, J. M. Heyes, J. Rosen, J. G. Chen, Y. Yan, F. Jiao, B. Xu, *J. Am. Chem. Soc.* **2017**, *139*, 3774–3783.
- [59] S. Zhu, B. Jiang, W. Bin Cai, M. Shao, *J. Am. Chem. Soc.* **2017**, *139*, 15664–15667.
- [60] Y. Hou, Y.-L. Liang, P.-C. Shi, Y.-B. Huang, R. Cao, *Appl. Catal. B Environ.* **2020**, *271*, 118929.
- [61] D. M. Koshy, S. Chen, D. U. Lee, M. B. Stevens, A. M. Abdellah, S. M. Dull, G. Chen, D. Nordlund, A. Gallo, C. Hahn, D. C. Higgins, Z. Bao, T. F. Jaramillo, *Angew. Chem. Int. Ed.* **2020**, *59*, 4043–4050.
- [62] N. Han, Y. Wang, L. Ma, J. Wen, J. Li, H. Zheng, K. Nie, X. Wang, F. Zhao, Y. Li, J. Fan, J. Zhong, T. Wu, D. J. Miller, J. Lu, S. T. Lee, Y. Li, *Chem* **2017**, *3*, 652–664.
- [63] T. Zheng, K. Jiang, N. Ta, Y. Hu, J. Zeng, J. Liu, H. Wang, *Joule* **2019**, *3*, 265–278.
- [64] S. Liu, H. Bin Yang, S. F. Hung, J. Ding, W. Cai, L. Liu, J. Gao, X. Li, X. Ren, Z. Kuang, Y. Huang, T. Zhang, B. Liu, *Angew. Chem. Int. Ed.* **2020**, *59*, 798–803.
- [65] H. Fei, J. Dong, Y. Feng, C. S. Allen, C. Wan, B. Voloskiy, M. Li, Z. Zhao, Y. Wang, H. Sun, P. An, W. Chen, Z. Guo, C. Lee, D. Chen, I. Shakir, M. Liu, T. Hu, Y. Li, A. I. Kirkland, X. Duan, Y. Huang, *Nat. Catal.* **2018**, *1*, 63–72.
- [66] X. Wang, W. Chen, L. Zhang, T. Yao, W. Liu, Y. Lin, H. Ju, J. Dong, L. Zheng, W. Yan, X. Zheng, Z. Li, X. Wang, J. Yang, D. He, Y. Wang, Z. Deng, Y. Wu, Y. Li, *J. Am. Chem. Soc.* **2017**, *139*, 9419–9422.
- [67] Y. Pan, R. Lin, Y. Chen, S. Liu, W. Zhu, X. Cao, W. Chen, K. Wu, W. C. Cheong, Y. Wang, L. Zheng, J. Luo, Y. Lin, Y. Liu, C. Liu, J. Li, Q. Lu, X. Chen, D. Wang, Q. Peng, C. Chen, Y. Li, *J. Am. Chem. Soc.* **2018**, *140*, 4218–4221.

## Entry for the Table of Contents



Nickel phthalocyanine molecules as active sites were installed into nickel-catecholate-linked 2D conductive metal-organic framework nanosheets for efficiently CO<sub>2</sub> electroreduction reaction with nearly 100% CO selectivity.